Sulfate soil stabilisation with binary blends of lime–silica fume and lime–ground granulated blast furnace slag

Ebailila Mansour [a], John Kinuthia [b], Jonathan Oti [b], Qusai Al-Waked [b, *]

[a] *Department of Civil Engineering, Faculty of Engineering, Bani Waleed University, Bani Waleed, Libya*
[b] *School of Engineering, Faculty of Computing, Engineering and Science, University of South Wales, Pontypridd CF37 1DL, UK*

ARTICLE INFO

ABSTRACT

The use of silica fume and ground granulated blast-furnace slag (GGBS) as a precursor to lime has been proven to be an effective sulfate soil stabilisation technique. However, which precursor is superior, in terms of both strength and swelling, is still questionable. Accordingly, the binary blends of lime–silica fume and lime–GGBS were separately added to pure kaolin soil and sulfate-dosed kaolin soil at a fixed combination dosage of 3L7S and 3L7GGBS. Then, a multi-scale investigation including unconfined compression strength (UCS), linear expansion, derivative thermogravimetric (DTG), X-ray diffraction and scanning electronic microscopy (SEM), was performed to assess their performance. The engineering tests indicated that the binary blends of lime–silica fume and lime–GGBS are effective in the stabilisation of non-sulfate and sulfate-dosed soil, with the former being superior in terms of the expansion and the latter being superior in terms of UCS. This disparity in performance is partly attributed to the higher calcium oxide content of 3L7GGBS which induces a relatively higher amount of ettringite, and partly due to the higher pozzolanic activity of silica fume which accelerates the consumption of lime and restricts the formation of ettringite on the expense of fabric modification.

Introduction

Calcium-based stabilisers such as lime are widely applicable stabilisers used for improving the reversible shrink-swell behaviour of expansive clays in civil engineering constructions, such as pavements and foundations [1]. However, there are significant concerns associated with lime production in terms of the higher energy consumption (4000 MJ/tonne), and the higher carbon dioxide emissions (800 Kg/tonne for L) emitted in the atmosphere [2]. Apart from that, lime also shows limited efficiency in the presence of sulfate, resulting in serious problems of expansion due to the nucleation and growth of ettringite [3,4], which forms due to the reaction between sulfate, calcium and alumina in the presence of water [5]. In this context, the use of industrial by-products as a partial replacement of lime, such as ground granulated blast-furnace slag-GGBS (a by-product of the steel industry) and silica fume-S (a by-product of the silicon and ferrosilicon alloy industries), has been encouraged.

In the presence of sulfate, the binary blend of lime–GGBS so far performed well and employed for several applications including soil stabilisation [6–11], durability improvement of flooded soils [12–14],

unfired bricks development [2,15–18], and heavy metal immobilisation [19,20]. Similarly, the binary blend of lime–silica fume has been investigated for several applications such as non-sulfate soil stabilisation [21,22], and sulfate soil stabilisation [23,24]. To mention a few, [9] studied the effect of various binary blends of lime-GGBS on the expansion and strength of kaolinite soil dosed with 4 % of gypsum and concluded that small addition of lime with GGBS can reduce the expansion with no significate compromise on the strength. [12] reported that the water absorption of Lower Oxford clay stabilised with a binary blend of lime-GGBS reduced as the GGBS content and the curing age increased. [13] found that a binary blend of 4L-12GGBS and 38 % of moisture content are the optimum conditions for restricting the expansion of Lower Oxford clay with 2 % of gypsum. [24] reported that the binary blend of 3L-7S is the optimum binder for suppressing the expansion of artificially high gypsum-dosed kaolinite, as it reduced the expansion from 32 % to 3.9 %.

Given the mentioned literature, it is obvious that regardless of the optimum blending ratio, designing an effective binder for sulfate soil stabilisation using either GGBS or Silica Fume as a partial replacement of lime is possible. However, the relevant literature in terms of the

---

comparison of the effect of lime–GGBS and lime–silica fume on the stabilisation of high sulfate soils to establish which of these binary blends is superior, has been vague and insufficient. This is clearly noticeable especially if the main variables affecting the performance of stabilised sulfate soil (such as the heterogeneity of soils, the concentration of sulfate and the amount of aluminium oxide content) were taken into consideration. For this reason, a comparative study considering the use of both GGBS and silica fume as a replacement of lime for sulfate soil stabilisation with a fixed sulfate concentration is needed to overcome this deficiency.

Accordingly, an attempt has been made in this study to compare the co-effect of lime–silica fume (LS) and lime–GGBS (LGGBS) blends in the stabilisation of non-sulfate and sulfate soil. Two binary blends (3L7S and 3L7GGBS) along with a control sole binder of 10*L* as a benchmark for comparison, were used to stabilise non-sulfate soil (pure kaolin) and artificial sulfate-dosed soil (kaolin + gypsum). Both mechanical (change in UCS) and physical (change in expansion) properties were examined to complement the present objective. The UCS performance has been investigated at different curing ages up to 90 days, while the expansion behaviour has been scrutinized throughout a prolonged soaking period of 200 days. The mechanism of alteration was also brought out clearly by performing micro-scale studies, including derivative thermogravimetric (DTG), X-ray diffraction and scanning electron microscopy (SEM) analysis.

Methodology

Materials

Five raw materials including kaolin (K) soil, gypsum (G), quicklime (L), ground granulated blast-furnace slag (GGBS) and silica fume (S), were used in this study. The kaolin soil (K) was in the form of a white fine powder, with a liquid limit of 56.7 %, a plastic limit of 33.3 % and a plasticity index of 23.4 %. It was supplied by Potterycrafts ltd, Stoke-on-Trent, UK, under a commercial trade name of China clay standard porcelain powder. The gypsum (G) was in the form of a fine white powder with a percentage purity of , and was obtained from Fisher Scientific ltd, Loughborough, Leicestershire, Leicester, UK. The quicklime (L) was in the form of an off-white fine powder, with a relative density of 3.31and was supplied by Tarmac Cement and Lime Company, Buxton Lime and Powders, Derbyshire, Derby, UK. The GGBS was in the physical form of very fine off-white powder and was supplied by Civil and Marine Slag Cement ltd, Llanwern, Newport, UK. The silica fume (S) was in the form of fine light grey amorphous power, with a silicon dioxide content (, 98.4 %). It was manufactured by Elkem Silicon Materials in Norway, and supplied by Tarmac Cement and Lime Campany, Buxton Lime and

Powders, Derbyshire, Derby, UK. Table 1 and Table 2 present the oxide compositions and the physical properties, respectively, while Fig. 1 plots the DTG curves of the raw materials.

Mix compositions and specimen preparation

The mix compositions assessed under this study (see Table 3) were designed using: 1) two target soil materials: pure kaolin soil and artificial sulfate-dosed soil (gypsum-dosed kaolin); and 2) three binder compositions (lime, lime–silica fume, lime–GGBS).

The artificial sulfate-dosed soil was made in the laboratory by blending kaolin with gypsum at a gypsum dosage of 9 % (equivalent to sulfate concentration of 4.2 %), by the mass of the dry target soil material (kaolin and gypsum). This artificial soil was used due to; 1) the homogeneity of kaolin structure, which eases the identification of complex interactions before embarking onto more complex soils; 2) the higher alumina content of kaolin, as it facilitates the formation of higher ettringite amount; and 3) gypsum is the most common source of sulfate encountered in natural soils. As for the choice of 9 % of gypsum which is equal to sulfate content of 4.2 %, this was based on the finding reported elsewhere [4], in which 9 % of gypsum was found to be the worst-case scenario for the expansion of kaolinite soil stabilised with lime content up to 6 wt%. Therefore, the adoption of 9 % stems from the hypothesis that if the comparison between the two blended binders was carried out using the worst sulfate scenario (high gypsum/alumina-enriched blended clay) for ettringite formation, then, any other scenario presented by any other sulfate soil is likely to be manageable to some reasonable degree.

As seen in Table 3, the total binder content was fixed at 10 % by the mass of the target soil materials, emulating the binder content used elsewhere [24,25]. This binder content was made at three different blending compositions; mainly 1) lime alone (10*L*) as a control; 2) lime–silica fume (3L7S) in line with the finding of the previous study [24]; and 3) lime–GGBS (3L7GGBS). Besides, the moisture content (MC) was set at 31 % for all the K- and K9G-based specimens. This fixed MC was equal to 1.1 times the optimum moisture content (OMC) for the control mix, which was obtained in accordance with BS EN 13286–2, 2012. The relatively higher MC was adopted because, in practice, the soil is always compacted at a relatively higher MC, in order to actualise the best performance [12–14].

For specimen preparation, initially, enough dry materials (soil and binder) were mixed in a mechanical mixer for 3 min. Thereafter, the water was introduced gradually, and the mixing continued for a further 3 min. The mixture was the poured into a steel mould (100-mm height and 50-mm diameter) and statically compressed employing a hydraulic jack as detailed elsewhere [24]. After compaction, the specimen was extruded using a plunger and wrapped in several runs of cling film. The

Table 1
Oxide composition of kaolin, lime, GGBS and silica fume.

Oxides	Compositions (%)			
	Kaolin	Lime	GGBS	Silica fume
	<0.01	71.56	37.99	0.2
	0.21	0.58	8.78	0.1
	47.32	0.67	35.54	98.4
	35.96	0.07	11.46	0.2
	0.07	<0.02	0.37	–
	0.12	0.03	0.02	0.03
	0.69	0.05	0.42	0.01
	0.02	0.02	0.43	–
	1.8	<0.01	0.43	0.2
	0.02	<0.01	0.7	–
	<0.01	0.02	0.04	–
	0.07	<0.01	0.09	–
	0.01	0.19	1.54	0.1
	0.1	–	–	–
	0.1	–	–	–
	13.1	27.4	2	0.5

Table 2
Particle size distribution and some other physical properties of the raw materials.

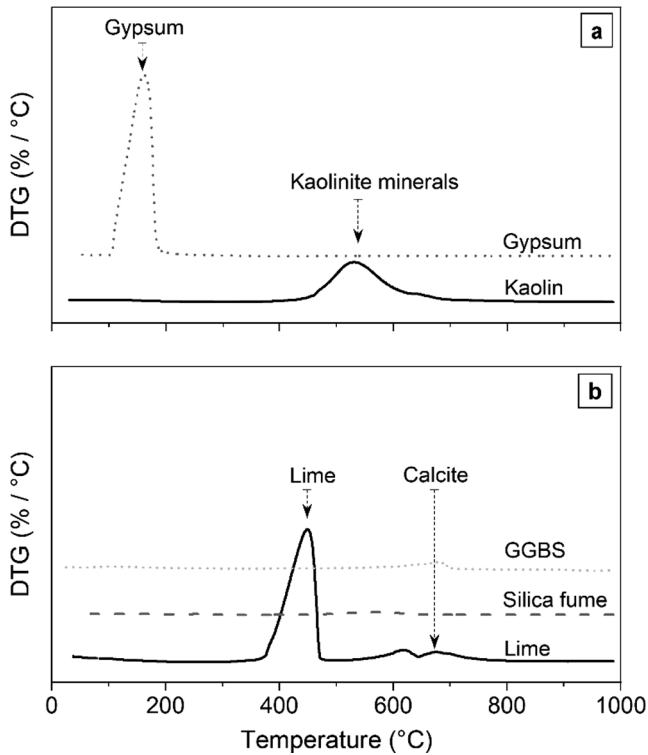| Properties	Kaolin	Lime	GGBS	Silica fume
Particle size distribution				
(mm)	0.012	0.35	0.025	0.1
(mm)	0.0085	0.25	0.02	0.04
(mm)	0.0062	0.06	0.007	0.025
(mm)	0.0018	<0.01	0.003	0.01
Other Properties				
Linear Shrinkage (%)	10.8	–	–	–
Linear Expansion (%)	6.2	–	–	–
Swelling Pressure (kPa)	1.3	–	–	–
Bulk density	–	480	1200	300
Specific gravity	2.14	2.82	2.9	3.15
Alkalinity value (pH)	5.37	12.62	10.4	7
Colour	White	White	Off-white	Grey

Fig. 1. Derivative thermogravimetric (DTG) curves of kaolin, gypsum, lime, silica fume and GGBS.

collected specimens were then sealed in an air-tight container, allowing for moist curing at a temperature of 20 2 °C until the date of testing. In total, eleven test specimens were fabricated for each mix, two of which were used for the expansion, and 9 specimens were used for testing the UCS at 7, 28 and 90 days of moist curing.

Testing method

Unconfined compression strength (UCS)

The UCS test was carried out using a Hounsfield Testing Machine, in accordance with BS EN ISO 17892–7:2018 [26,27], at a strain ratio of 2 mm per minute, in line with [12–14]. Three specimens per mix composition after each of the prescribed curing period (7, 28 and 90 days) was tested, and the mean was used as the representative UCS.

Swelling behaviour

The swelling behaviour was examined by means of linear expansion measurement, in accordance with [28], using perspex cells (see Fig. 2), in line with [9,11,13,18,29]. The expansion measurement was carried out in replicate and commenced after 7 days of moist curing. Immediately, after 7 days of moist curing, 10 mm of the top and bottom of two specimens per mix composition were unwrapped and placed on a porous

disc located in a perspex cell as schematically shown in Fig. 2. Thereafter, the perspex cells were covered with lids, equipped with digital dial gauges to measure the vertical displacement (change in height) of the cylinders. On the completion of the initial reading, the water was carefully added to the perspex cells, through the upper inlet, until the exposed 10 mm-bottom part of the specimens was submerged in water, while keeping the water level constant through the experimentation period, to ensure no water evaporation from the specimens has occurred. This water level was adopted because it has been used by several researchers [9,11,13,18,29]. This process was followed by recording the dial gauge reading on a daily basis for the initial 28 days (rapid swelling period), and then random reading for the rest of the soaking period was carried out for a better presentation of the graphs. The average of the two measurements (changes in height) was reported as the representative change in height. Finally, the ratio of the change in height to the original height was reported as the representative expansion. A third test was sometimes necessary, especially when the variation of the change in height of the first two specimens differed by 5 % of the average (normally a variation of was observed).

Mineralogical and analytical tests

The thermal, mineralogical, and microstructural analyses were operated on a randomly oriented portion of pieces collected from the fractured UCS and expansion specimens. Prior to testing, the randomly oriented portions, were dried in a desiccator at with the aid of silica gel to prevent hydration, and then milled and sieved through a 0.074 mm sieve. Consequently, the mineralogical and analytical tests including
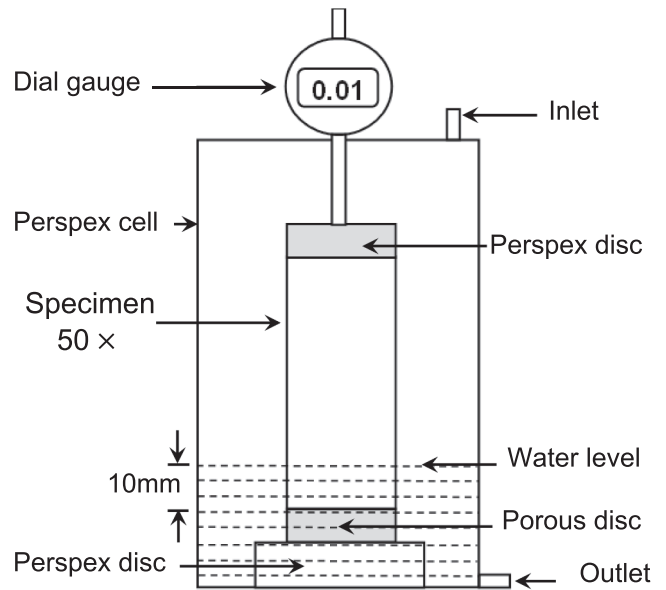

Fig. 2. Schematic diagram of a perspex cell test set-up used for linear expansion measurement.

Table 3
Mix design using pure kaolin and artificial sulfate-dosed kaolin.

Mix Code	Mix compositions (%)						
	Target Soil Materials (%)		Water (%)	Binder (%)	Binder composition in % by Target Soil Material mass		
	Kaolin	Gypsum			Lime	Silica fume	GGBS
K–10L	100	–	31	10	10	–	–
K–3L7S	100	–	31	10	3	7	–
K–3L7GGBS	100	–	31	10	3	–	7
K9G–10L	91	9	31	10	10	–	–
K9G–3L7S	91	9	31	10	3	7	–
K9G–3L7GGBS	91	9	31	10	3	–	7

derivative thermogravimetric analysis (DTG), X-ray diffraction analysis (XRD) and scanning electron microscopy analysis (SEM), were conducted as follows. The derivative thermogravimetric (DTG analysis) was conducted using a TA instruments TGA55 kit. The DTG analysis was operated from room temperature up to 1000 °C, under an argon atmosphere, at a flow heating rate of 20 . The mineralogical crystal phases (XRD patterns) were established using a STOE powder diffraction system. The XRD scans were operated using radiation at an angle scan (two theta) ranging from 10 to 84, at a wavelength (λ) of 1.540598 Å, step size of , and copper generating settings of 40 kV and 40 mA. The microstructure was inspected using JSM-7900F Schottky field emission scanning electron microscopy (FE–SEM). The FE-SEM analysis was operated at a lower accelerating voltage of 5 kV to perform high-resolution imaging at different magnifications ranging up to 30000x.

Results

Unconfined compressive strength (UCS)

Fig. 3 presents the UCS development of pure kaolin (K) and artificial sulfate-dosed kaolin (K9G) specimens stabilised with 10 wt% of lime alone (10*L*), lime–silica fume (3L7S) and lime–GGBS (3L7GGBS) at 7, 28 and 90 days moist curing period. In general, all the formulations exhibited a steady increase in strength development at all the prescribed moist curing ages, with a higher strength gain ratio (increase in strength relative to the proceeding curing age) being pronounced for all the sulfate-dosed specimens at all the moist curing ages.

In the case of the pure kaolin system in which no sulfate was introduced, the sequential order (from high to low) of the 7-days UCS, followed the binder sequence of 10*L* > 3L7S > 3L7GGBS, where lime alone yielded the highest strength of 607 and 3L7GGBS experienced the lowest strength of 407 . At 28 days of hydration, the binder sequence was changed, where 3L7S produced the highest UCS of 800 and 10*L* yielded the lowest UCS of 720 , with a strength gain ratio (relative to its 7-days counterparts) of 60 % and 19 %, respectively. This strength trend, therefore, signifies the superiority of 3L7S at the early-term curing age (>28 days), which was expected due to the higher pozzolanic activity of silica fume, relative to that of GGBS. However, at 90-days of curing, the strength trend was further changed, where 3L7GGBS demonstrated the highest strength of 1482 and 10*L* yielded the lowest 90-days UCS of 839 , with strength gain ratio (relative to its 28-days counterparts) of 89 % and 16 %, respectively. This suggests that 3LGGBS exhibited better performance than both 3L7S and 10*L* over a prolonged curing period of 90 days in the absence of sulfate.

As for the case of the artificial sulfate kaolin (K9G), it was observed that the strength trend at all the curing ages was in accord with the sequence of binder domination obtained in the absence of sulfate (K) at 90 days (10*L* < 3L7S < 3L7GGBS), but with an increased strength value. In this regard, the control binder (10*L*) produced the lowest 90-day strength of 1995 , the binary blend of 3L7S yielded a medial 90-day strength of 2100 , while the binary blend of 3L7GGBS experienced the highest 90-day strength of 2828 . Therefore, in the light of this information, it can be eventually inferred that the binary blend of 3L7GGBS is superior to that of 3L7S in terms of the UCS in both the absence and the presence of sulfate.

Linear expansion

The typical linear expansion plots, recorded through a soaking period of 200 days, for pure kaolin (K) and artificial sulfate-dosed kaolin (K9G) specimens stabilised with 10*L*, 3L7S and L7GGBS blends at a fixed binder dose of 10 wt%, are shown in Fig. 4.

In the absence of sulfate, the result shown in Fig. 4a indicated that there was a marginal difference between the expansion of the three mixes. The control mix (K–10*L*) experienced a maximum expansion of 5 %, as opposed to that of 3.4 % for K–3L7GGBS and 3 % for K–3L7S. This
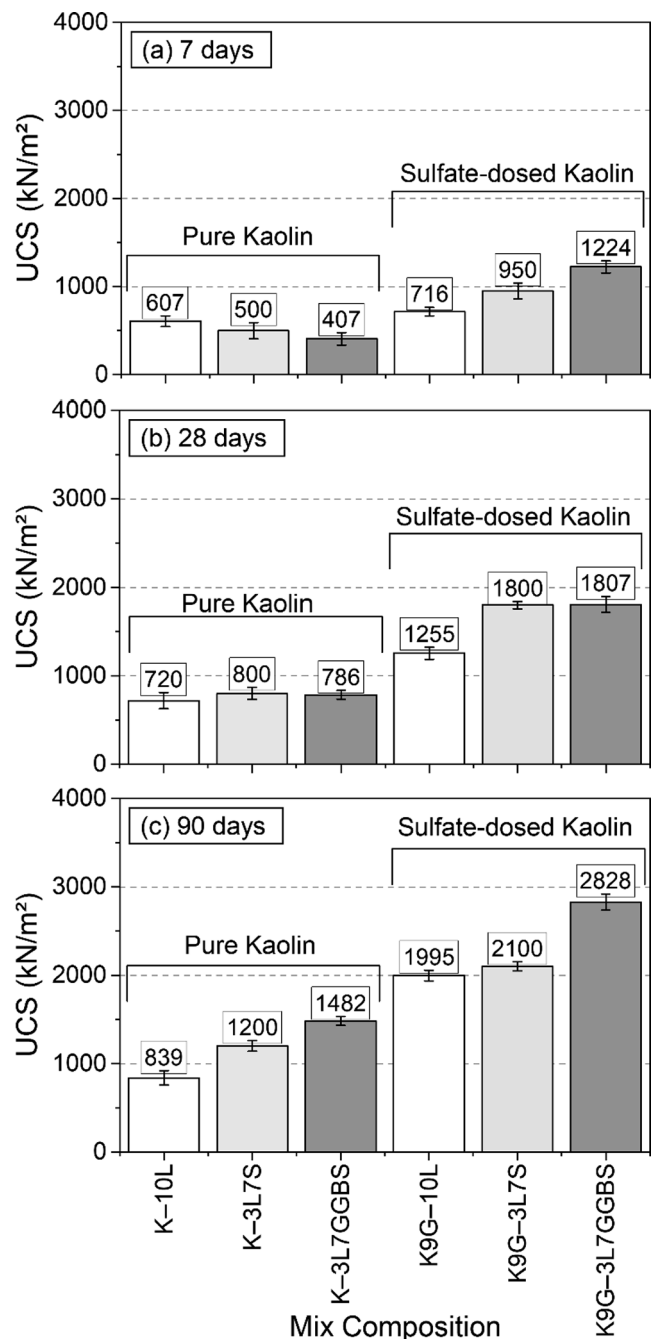

Fig. 3. UCS of pure kaolin (K) and artificial sulfate-dosed kaolin (K9G) stabilised with 10 wt% of lime alone (10*L*), lime–silica fume (3l7S) and lime–GGBS (3L7GGBS) at; a) 7-days, b) 28-days and 90-days moist curing.

expansion occurred immediately after soaking in water, with about 90 % of the ultimate expansion occurring within the first three days of soaking. However, this expansion trend was not the case in the presence of sulfate (K9G), as there was a staggering expansion development for the artificial sulfate specimens, making a noticeable difference among the blended binders investigated. In this context, the sole addition of lime (10*L*) yielded the highest expansion of 32 %, while the 3L7GGBS induced a moderate expansion of 7 % and the 3L7S demonstrated the lowest expansion of 4 %. This indicates the superiority of 3LS in terms of the suppression of the expansion of sulfate soils. It also suggests that the expansion induced by the introduction of gypsum was not completely suppressed by the binary blends of 3L7S and 3L7GGBS, as there was a slight increase in the range of 1 to 4 % in the expansion of K9G–3L7S and
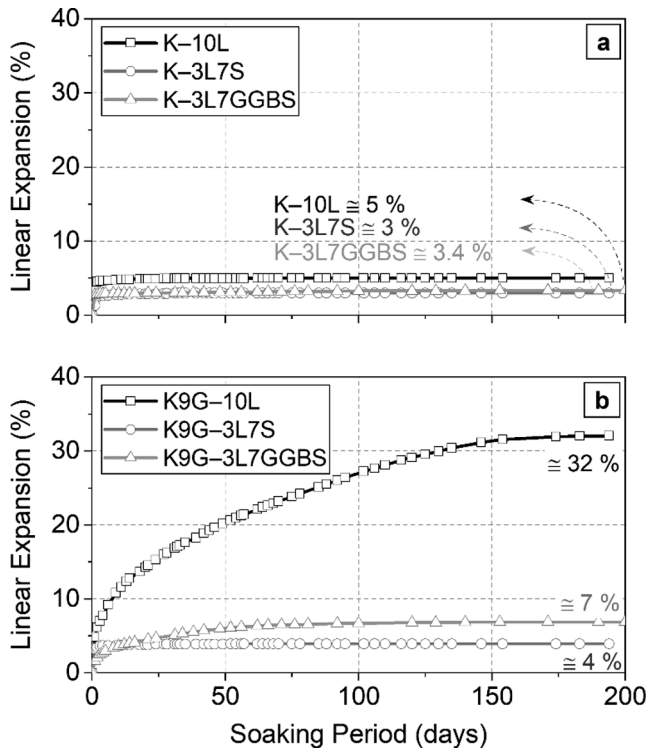
Fig. 4. Typical 200-days expansion trends of (a) pure kaolin (K), and (b) artificial sulfate-dosed kaolin (K9G), stabilised with 10 wt% of lime alone, lime–silica fume and lime–GGBS.

K9G–3L7GGBS, relative to their counterparts of K–3L7S and K–3L7GGBS.

Derivative-thermogravimetric analysis (DTG)

The DTG curves of pure kaolin and artificial sulfate-dosed kaolin specimens stabilised with 10 wt% of 10*L*, 3L7S and 3L7GGBS after 7 days of moist curing, are presented in Fig. 5, alongside explanatory notes for the major peaks.

For K series specimens, the DTG curves (see Fig. 5a) showed one additional endothermic transition zones in the range of (portlandite), in addition to that appeared in the parent kaolin at a temperature range of . This portlandite peak signifies the incomplete consumption of lime during the first 7 days of moist curing. The intensity of the portlandite peak was, however, noted to be reduced on the substitution of lime with GGBS as shown by K–3L7GGBS and completely disappeared in the case of lime–silica fume blend as given by K–3L7S. As for the K9G series specimens, the main endothermic peaks identified were: 1) ettringite peak at due to the dehydration of water molecules of the ettringite, 2) gypsum peak at due to the dehydration of gypsum, 3) portlandite peak at due to dihydroxylation of non-consumed , and 4) kaolinite peak at due to the dihydroxylation of kaolinite minerals. The ettringite peak appeared relatively blunter in specimens stabilised with 10*L* and 3L7GGBS, and hardly visible in the case of 3L7S. This suggests that 3L7S was superior to 3L7GGBS in restricting the ettringite formation. This suggestion was also strengthened by the intensity of the gypsum peak, it appeared relatively sharper in the case of K9G–3L7S, implying that the K9G–3L7S system consumed a lesser gypsum amount during the reaction.

X-ray diffraction (XRD)

Fig. 6 compares the X-ray diffractograms of sulfate kaolin (K9G) specimens stabilised with 10 wt% of lime alone (10*L*), lime–silica fume (3L7S) and lime–GGBS (3L7GGBS) at 90-days of moist curing.
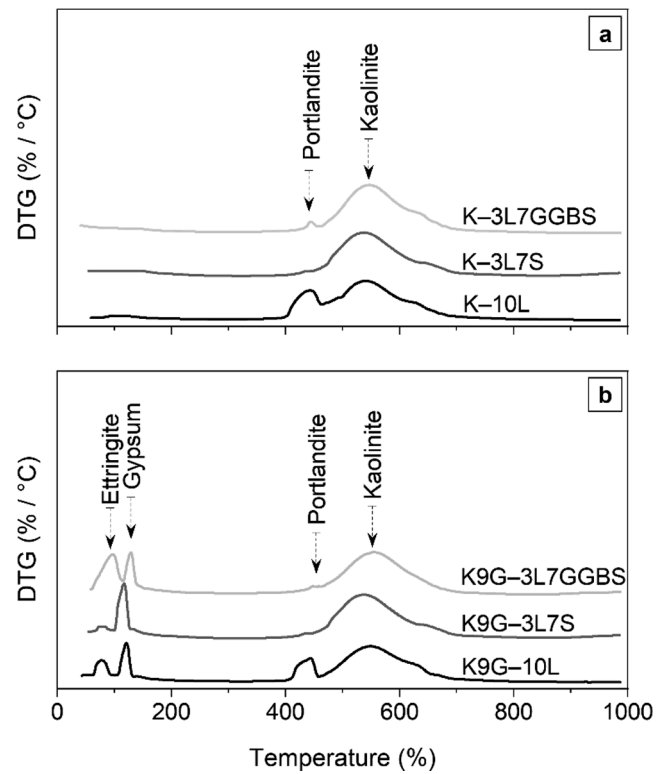

Fig. 5. The 7-day DTG curves of (a) pure kaolin (K), and (b) artificial sulfate-dosed kaolin (K9G), stabilised with 10 wt% of lime alone, lime–silica fume and lime–GGBS.
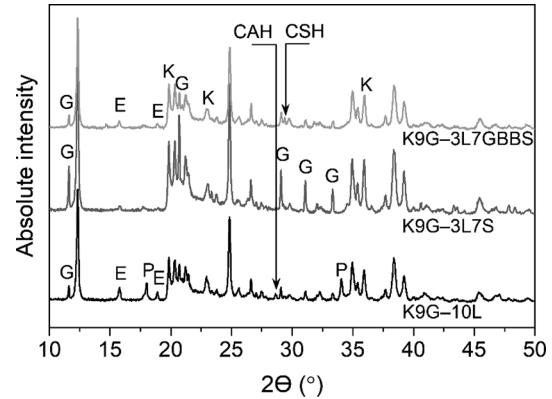

Fig. 6. The 90-day XED curves of artificial sulfate-dosed kaolin (K9G), stabilised with 10 wt% of lime alone, lime–silica fume and lime–GGBS.

The main minerals identified in the X-ray diffraction were kaolinite–K, quartz–Q, gypsum–G, ettringite–E, portlandite–P, calcium silicate hydrate–CSH, and calcium aluminate hydrate–CAH. The intensity of kaolinite reflection (at 2θ = 12.3°, 19.8°, 21.2°, 23°, 24.8°, 34.9°, 35.9°, 38.4° and 39.2°) appeared to be increased on the substitution of lime with silica fume as given by K9G–3L7S. This is probably because silica fume promotes more nucleation sites at an earlier age, accelerating the hydration reactions [30], thereby the binder induces lesser soil particle modification. In such a case, the less flocculated particles tend to exhibit higher reflection intensities owing to the increase of incident rays compared to their well-flocculated particles [31].

The quartz reflection (at) appeared stable in all the X-ray diffractograms. The intensity of portlandite reflection (at 18.08°) disappeared in the binary systems (K9G–3L7GGBS and K9G–3L7S) and appeared sharper in K9G–10*L*, the existence of which indicates a surplus supply of

lime. The ettringite reflections (at 15.8° and 18.9°) appeared sharper in the case of K9G–10L and K9G–3L7GGBS, and relatively lower in the case of K9G–3L7S. Conversely, the gypsum reflections (at 2θ = 11.6°, 20.7°, 29.1°, 31.1° and 33.3°) moved contrariwise, all of which reflect those of DTG curves. As for the hydrated products, the CSH reflection was only detected (at in line with [32,33]) in the XRD pattern of K9G–3L7S, whereas the CAH reflection (at in line with [34]) was noticed in the XRD pattern of the control mix (K9G–10L). Keeping this along with that of kaolinite reflections in view, it can be inferred that silica fume affects the hydration kinetics by promoting more nucleation sites on the expense of fabric modification. Therefore, it accelerates the hydration reactions, speeding up the consumption of calcium ions, reducing the solubility rate of alumina, and promoting the formation of CSH over that of CAH.

Field-emission scanning electron microscopy (FE-SEM)

Fig. 7 elaborates the microstructure morphology, at the 200th-day water soaking condition, for the artificial sulfate-dosed specimens stabilised with 10 wt% of lime (10L) and binary blends of lime–silica fume (3L7S) and lime–GGBS (3L7GGBS).

As seen in Fig. 7, the FE–SEM images revealed the existence of plate-like particles of kaolinite, small globular-like particles with no definite shapes and needle-like structures with different morphologies. In the case of the hydrated products, the higher magnification (X30k) of FE–SEM images indicated that, in the 10L0S system, the globular-like particles of hydrated products possess a clumped cluster form (mostly on the edge of soil particles) with no definite shapes. In contrast, the hydrated products of 3L7S and 3L7GGBS appeared in a well-distributed form with globular-like particles. The difference is probably attributed to the fineness and pozzolanic activity of silica fume and GGBS, as it induces more nucleation sites for the formation of hydrated products, which correspondingly leads to the formation of less clumped forms of hydrated products. As for the case of the needle-like structures, the FE–SEM revealed that the needles possess a different morphology; a long circular and columnar morphology for the case of K9G–10L and pencil-shaped hexagonal crystals in the case of K9G–3L7GGBS. These needles which are commonly reported as ettringite crystals were absent in K9G–3L7S. In crystallography, the ettringite possesses a hexagonal prismatic shape, similar to that appeared in K9G–3L7GGBS, rather than a long circular and columnar morphology as the one that appeared in K9G–10L. Therefore, the needles presented in K9G–10L0S are probably due to the remained crystals of ettringite after carbonation or the crystals of aragonite resulting from ettringite carbonation, thus, further research along this line is recommended to validate.

Discussion

Prior to stabilisation, clay soils in their natural state, are a relatively malleable compacted mixture of negatively charged particles [9]. Therefore, on water soaking, the negatively charged surfaces of clay particles attract water molecules, thereby altering the electrochemical interparticle force equilibrium. This attraction leads to expansion via a mechanism known as an inter-crystalline expansion [35]. In the case of quicklime, the first reaction taking a place is lime hydration, which creates heat and dries out the soil through the action of slaking. At the end of this reaction, quicklime is hydrated, resulting in hydrated lime, which in turn dissolves, realising calcium ions. In the absence of sulfate, the calcium ions fix to the surface of soil particles, replacing most of the exchangeable ions [36]. This replacement in ions balances the electrostatic charges of soil particles [5] and promotes different soil particles arrangement [37], a process known as flocculation and agglomeration of soil particles [38,39]. Besides the release of , the hydroxides (OH) are also presented, causing a significant increase in the pH value up to about 12.4 [38]. This increase in the pH aids the dissolution of aluminate (Al) and silicate (Si) ions in soil sheets. This then enables the formation of pozzolanic reactions between the excess calcium from lime and dissolved (Al and Si) ions from treated soil [2]. These pozzolanic reactions produce different hydrated products, of which calcium silica hydrate (CSH), calcium aluminate hydrate (CAH) and a mixture of these gel categories (calcium alumino silica hydrate (CASH)) are typically formed
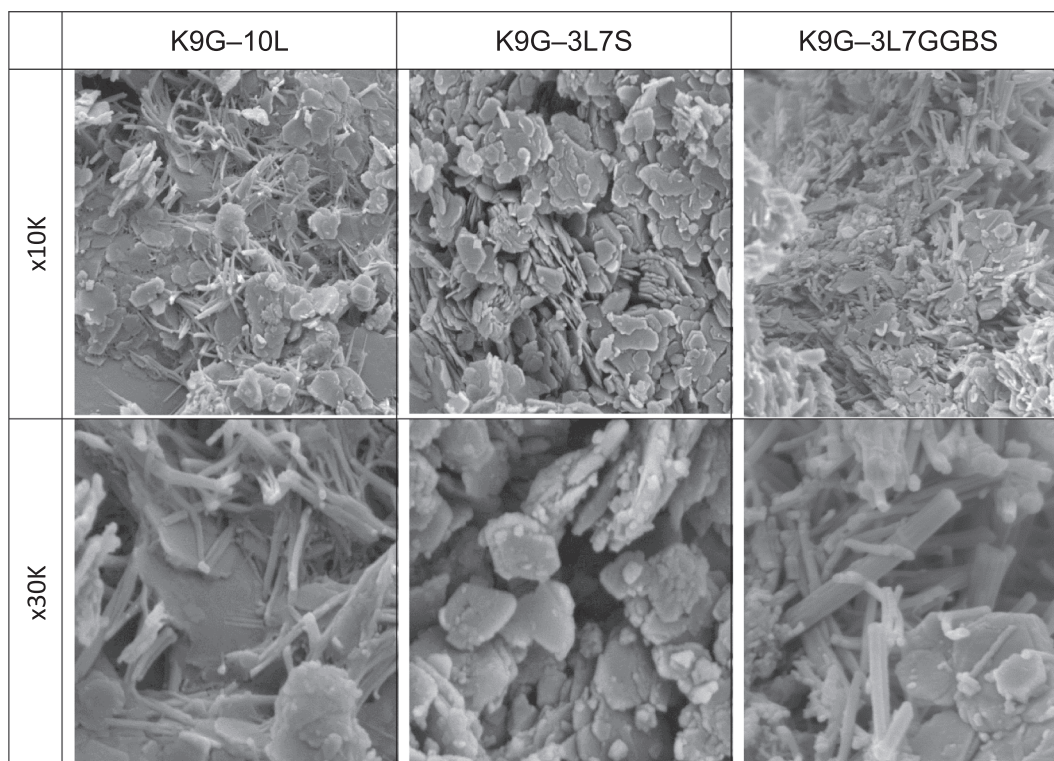

Fig. 7. The FE-SEM images of artificial sulfate-dosed kaolin (K9G) stabilised with 10 wt% of lime alone (10L), lime–silica fume (3L7S) and lime–GGBS (3L7GGBS).

[29]. However, only those CSH and CAH hydrates were detected in the X-ray diffractograms of the current study, the absence of which is probably attributed to the overlapping with kaolinite reflections.

Following the pozzolanic reaction, portlandite () may also remain as was detected in the DTG and XRD patterns of K–10*L* under this study. The presence of portlandite crystals is not favoured, as they prevent the dissolution of kaolinite minerals [40], and reduces the cohesion of the system [41], all of which induce a compromise on strength. However, on the substitution of lime with pozzolanic materials such as silica fume or GGBS, the reverse phenomenon associated with portlandite can be revoked, contributing to a higher degree of strength. This is because these pozzolanas promote more nucleation sites at earlier hydration age [30], thereby accelerating the consumption of and promoting the formation of more hydrates (CSH and CAH). The hydrated products induce pore-blocking effect and system densification, all of which contribute to the stability of the system under soaking condition [13], justifying the lower expansion of K–3L7S and K–3L7GGBS relative to that of K–10*L*. Therefore, in summary, the main reactions involved in lime soil stabilisation in the absence of sulfate are short-term reactions (ion exchange and flocculation-agglomeration of soil particles), and long-term reactions (pozzolanic reactions) [38,39]. However, the presence of sulfate () can cause a significant influence on the short-term reaction, with the formation of ettringite [42].

The ettringite is a highly hydrated crystalline mineral produced due to the reaction between the soluble sulfate, calcium (from lime) and alumina (from the soil) in the presence of water [43,44]. At earlier moist curing age (7-days), the amount of soluble sulfate is limited due to the relatively low solubility of gypsum and the unavailability of enough moisture content for the complete dissolution of gypsum, thus, only limited ettringite crystals would form [35]. These ettringite crystals grow within soil pores in the form of very small needle-like and colloidal crystals [45], with a long columnar morphology as detected in the FE–SEM images. Prior to soaking, the nucleation and growth of ettringite are beneficial, as it improves the strength through; 1) the reduction of porosity of the host matrix, 2) the formation of extensive crystals interlocking due to growth of ettringite around the soil particles, and 3) the dewatering of the system due to the high-water absorption of ettringite [24,46]. This, therefore, is in support of why K9G–specimens yielded superior strength performance than those of K–based specimens (see Fig. 3).

Upon soaking, the movement of water within the stabilised soil tends to solubilise the unconsumed ingredients and acts as an avenue for ion migration and hence, becomes a source of ions supply at the nucleation sites of ettringite [24,35]. This then results in the formation of extensive ettringite [47], which could not be accommodated within the system pores [48]. These ettringite crystals have a higher specific surface area with unbalanced surface charges, inflicting bipolar water molecules attraction [16], and hence the orientation of water molecules to mitigate their surface energy. This action is believed to lead to the formation of an electric double layer around the crystals of ettringite, where the water layer builds up with time to multimolecular water layers [49]. This action is commonly referred to as ettringite crystalline swelling. The ettringite crystalline swelling can cause a drastic expansion [8,50], which was also confirmed in this study by the higher expansion (32 %) of K9G–10*L*, relative to 5 % for K–10*L*. However, with the incorporation of silica fume or GGBS in the system, these pozzolans affect the hydration kinetics by promoting more nucleation sites at earlier hydration age [30,51]. These additional nucleation sites provide a competitive consumption of , thereby inhibiting the formation of ettringite [52], which was also confirmed by both DTG and XRD patterns.

Apart from the ettringite restriction, the incorporation of silica fume or GGBS can also form further hydrated products, depleting the constituents required for the formation of ettringite [47], and inducing a pore-blocking effect [12]. The blockage of the capillary pores induces permeability reduction and porosity enhancement [29], both of which contribute to strength and expansion improvement [24]. Thus, sulfate-dosed specimens made with binary blends of lime–silica fume (K9G–3L7S) and lime–GGBS (K9G–3L7GGBS), in general, experienced a drastic reduction in expansion. However, the observation of this current study indicated that lime–silica fume blend exhibited superior expansion performance, while lime–GGBS out-performed in terms of the UCS. This disparity in performance can be partly attributed to the higher calcium oxide content of 3L7GGBS, suggesting the formation of a higher amount of ettringite (which was also confirmed by the DTG, XRD and FE-SEM analysis). Therefore, a higher degree of strength gain associated with ettringite has occurred in 3L7GGBS, relative to that of 3L7S.

The higher pozzolanic activity of silica fume is also a contributing factor to the relatively lower UCS of the 3L7S–based mix as compared to 3L7GS. According to [53], the un-densified silica fume had higher pozzolanic activity than GGBS, where it can yield calcium hydroxide consumption up to four times higher than that of GGBS. This indicates that the hydration reaction of lime–silica fume blend is more rapid than lime–GGBS reaction, which would lead to a faster depletion of the main components responsible for ettringite formation. This restriction phenomenon would make the system chemically more stable under soaking condition, as confirmed by the linear expansion of K9G–3L7S relative to that of K9G–3L7GGBS. On the other hand, the accelerating reaction would negatively affect the short-term reactions (ion exchange and flocculation-agglomeration of soil particles) due to the faster exhausting of lime, which agreed with the microstructure of the K9G–3L7S specimen. This negative effect would induce a lower degree of strength gain associated with the fabric modification, justifying the relatively lower 90-days strength of 2100 for K9G–3L7S, as compared to that of 2828 for K9G–3L7GGBS.

Overall, the outcome of this comparative study suggested that the binary blends of lime–silica fume and lime–GGBS are effective soil stabilisers, of which the former was superior in terms of the expansion while the latter was superior in terms of the UCS. Therefore, to achieve optimal performance, an attempt to optimise the ternary blends of lime-GGBS-silica fume is recommended to maximise the benefits of each.

Conclusions

The main conclusions can be drawn as follows:

1. The presence of sulfate increases the UCS and swelling of kaolin specimens stabilised with 10*L*, 3L7S and 3L7GGBS, due to the formation of ettringite. Under moist curing, the ettringite improves the UCS through the reduction of the porosity, interlocking of the matrix and the dewatering of the system. In contrast, in underwater soaking, the ettringite attracts water molecules, thus causing a drastic swelling.

2. The addition of 3L-7S and 3L-7GGBS in both non-sulfate and sulfate-dosed kaolin soil yielded lower swelling magnitude than the sole addition of lime (10*L*). This is because silica fume and GGBS provide more nucleation sites, which induces a faster depletion of the main components responsible for the formation of ettringite, and forms more hydrated products.

3. The sole addition of lime – 10*L* achieved the highest 7-days UCS, while the binary blend of 3L7S and 3L7GGBS induced the highest 28-days UCS and the highest 90-days UCS, respectively.

4. Over prolonged curing period, the binary blend of 3L-7GGBS yielded the highest UCS, while 3L7S induced the lowest swelling, in the absence and the presence of sulfate. The superiority of 3L-7GGBS in UCS is due to the higher degree of fabric modification and the formation of a higher amount of ettringite, as opposed to that of the 3L-7S system, which induces a lower degree of fabric modification and lower amount of ettringite, facilitating the suppression of the swelling.

5. The limitations of this study that could affect the authenticity of the findings of the laboratory experiments are the utilisation of an

artificial sulfate-dosed soil (kaolin and gypsum) and a fixed binder dosage of 10 % by the mass of the soil.

Overall, it can be stated that the use of binary blends of 3L–7S and 3L–7GGBS for sulfate soil stabilisation are promising effective stabilisation method, with the former being superior in terms of the expansion while the latter is superior in terms of the UCS. Consequently, further efforts and research are needed to establish the optimal ternary blends of lime-GGBS-silica fume with the overall aim of maximising the benefits of these stabilisers.

CRediT authorship contribution statement

Mansour Ebailila: Conceptualization, Methodology, Software, Data curation, Investigation, Validation, Writing – original draft, Visualization. **John Kinuthia:** Conceptualization, Supervision, Validation, Project administration. **Jonathan Oti:** Supervision, Project administration, Validation, Visualization. **Qusai Al-Waked:** Writing – review & editing, Validation.

Declaration of Competing Interest

The authors declare that they have no known competing financial interests or personal relationships that could have appeared to influence the work reported in this paper.

Data availability

Data will be made available on request.

References

[1] Puppala AJ. Advances in ground modification with chemical additives: From theory to practice. Transp Geotech 2016;9:123–38. https://doi.org/10.1016/j.trgeo.2016.08.004.

[2] Oti JE, Kinuthia JM, Bai J. Unfired clay bricks: from laboratory to industrial production 2009;4:229–37. https://doi.org/10.1680/ensu.2009.162.

[3] Aldaood A, Bouasker M, Al-Mukhtar M. Free swell potential of lime-treated gypseous soil. Appl Clay Sci 2014;102:93–103. https://doi.org/10.1016/j.clay.2014.10.015.

[4] Ebailila M, Kinuthia J, Oti J. Role of Gypsum Content on the Long-Term Performance of Lime-Stabilised Soil. Materials 2022;15:5099. https://doi.org/10.3390/ma15155099.

[5] Nidzam RM, Kinuthia JM. Sustainable soil stabilisation with blastfurnace slag – a review. Proceedings of the Institution of Civil Engineers - Construction Materials 2010;163(3):157–65.

[6] Seco A, Ramírez F, Miqueleiz L, Garci B, Prieto E. The use of non-conventional additives in Marls stabilization. Appl Clay Sci 2011;51:419–23. https://doi.org/10.1016/j.clay.2010.12.032.

[7] Seco A, Ramírez F, Miqueleiz L, García B. Stabilization of expansive soils for use in construction. Appl Clay Sci 2011;51:348–52. https://doi.org/10.1016/j.clay.2010.12.027.

[8] Seco A, Miqueleiz L, Prieto E, Marcelino S, García B, Urmeneta P. Sulfate soils stabilization with magnesium-based binders. Appl Clay Sci 2017;135:457–64. https://doi.org/10.1016/j.clay.2016.10.033.

[9] Wild S, Kinuthia JM, Robinson RB, Humphreys I. On the strength and swelling properties of lime-stabilized kaolinite in the presence of sulphates. Clay miner 1996;31(3):423–33.

[10] Wild S, Kinuthia JM, Jones GI, Higgins DD. Effects of partial substitution of lime with ground granulated blast furnace slag (GGBS) on the strength properties of lime-stabilised sulphate-bearing clay soils. Eng Geol 1998;51(1):37–53.

[11] S. Wild, J.M. Kinuthia, G.I. Jones, D.D. Higgins, Suppression of swelling associated with ettringite formation in lime stabilized sulphate bearing clay soils by partial substitution of lime with ground granulated blastfurnace slag, 1999. 10.1016/S0013-7952(98)00069-6.

[12] Obuzor GN, Kinuthia JM, Robinson RB. Enhancing the durability of flooded low-capacity soils by utilizing lime-activated ground granulated blastfurnace slag (GGBS). Eng Geol 2011;123:179–86. https://doi.org/10.1016/j.enggeo.2011.07.009.

[13] Obuzor GN, Kinuthia JM, Robinson RB. Utilisation of lime activated GGBS to reduce the deleterious effect of flooding on stabilised road structural materials: A laboratory simulation. Eng Geol 2011;122:334–8. https://doi.org/10.1016/j.enggeo.2011.06.010.

[14] Obuzor GN, Kinuthia JM, Robinson RB. Soil stabilisation with lime-activated-GGBS-A mitigation to flooding effects on road structural layers/embankments constructed on floodplains. Eng Geol 2012;151:112–9. https://doi.org/10.1016/j.enggeo.2012.09.010.

[15] Oti JE, Kinuthia JM, Bai J. Engineering properties of unfired clay masonry bricks. Eng Geol 2009;107:130–9. https://doi.org/10.1016/j.enggeo.2009.05.002.

[16] Oti JE, Kinuthia JM, Bai J. Compressive strength and microstructural analysis of unfired clay masonry bricks. Eng Geol 2009;109:230–40. https://doi.org/10.1016/j.enggeo.2009.08.010.

[17] Oti JE, Kinuthia JM. Stabilised unfired clay bricks for environmental and sustainable use. Appl Clay Sci 2012;58:52–9. https://doi.org/10.1016/j.clay.2012.01.011.

[18] Oti JE, Kinuthia JM, Robinson RB. The development of unfired clay building material using Brick Dust Waste and Mercia mudstone clay. Appl Clay Sci 2014;102:148–54. https://doi.org/10.1016/j.clay.2014.09.031.

[19] Jin F, Al-Tabbaa A. Evaluation of novel reactive MgO activated slag binder for the immobilization of lead and zinc. Chemosphere 2014;117:285–94. https://doi.org/10.1016/j.chemosphere.2014.07.027.

[20] Wang F, Wang H, Jin F, Al-Tabbaa A. The performance of blended conventional and novel binders in the in-situ stabilisation/solidification of a contaminated site soil. J Hazard Mater 2015;285:46–52. https://doi.org/10.1016/j.jhazmat.2014.11.002.

[21] Saygili A, Dayan M. Freeze-thaw behavior of lime stabilized clay reinforced with silica fume and synthetic fibers. Cold Reg Sci Technol 2019;161:107–14. https://doi.org/10.1016/j.coldregions.2019.03.010.

[22] GhavamShirazi S, Bilsel H. Characterization of volume change and strength behavior of micro-silica and lime-stabilized Cyprus clay. Acta Geotech 2021;16:827–40. https://doi.org/10.1007/s11440-020-01060-1.

[23] N. Moayyeri, M. Oulapour, A. Haghighi, Study of geotechnical properties of a Gypsiferous soil treated with lime and silica fume, Geomechanics and Engineering. 17 (2019) 195–206. 10.12989/gae.2019.17.2.195.

[24] Ebailila M, Kinuthia J, Oti J. Suppression of Sulfate-Induced Expansion with Lime-Silica Fume Blends. Materials 2022;15:2821. https://doi.org/10.3390/ma15082821.

[25] Li W, Yi Y, Puppala AJ. Suppressing Ettringite-Induced Swelling of Gypseous Soil by Using Magnesia-Activated Ground Granulated Blast-Furnace Slag. J Geotech Geoenviron Eng 2020;146:06020008. https://doi.org/10.1061/(asce)gt.1943-5606.0002292.

[26] BS 1924–2, Hydraulically bound and stabilized materials for civil engineering purposes — Part 2: Sample preparation and testing of materials during and after treatment, BSI Standards Limited, London, UK, 2018.

[27] BS EN ISO 17892-7, Geotechnical investigation and testing-Laboratory testing of soil — Part 7: Unconfined compression test (ISO 17892-7:2017), BSI Standards Limited, London, UK, 2018.

[28] BS EN 13286-49, Unbound and hydraulically bound mixtures — Part 49: Accelerated swelling test for soil treated by lime and/or hydraulic binder, BSI Standards Limited, London, UK, 2004.

[29] Kinuthia JM, Nidzam RM. Towards zero industrial waste: Utilisation of brick dust waste in sustainable construction. Waste Manage 2011;31:1867–78. https://doi.org/10.1016/j.wasman.2011.03.020.

[30] Xu Z, Zhou Z, Du P, Cheng X. Effects of nano-silica on hydration properties of tricalcium silicate. Constr Build Mater 2016;125:1169–77. https://doi.org/10.1016/j.conbuildmat.2016.09.003.

[31] Goodarzi AR, Akbari HR, Salimi M. Enhanced stabilization of highly expansive clays by mixing cement and silica fume. Appl Clay Sci 2016;132–133:675–84. https://doi.org/10.1016/j.clay.2016.08.023.

[32] Keramatikerman M, Chegenizadeh A, Nikraz H. Effect of GGBFS and lime binders on the engineering properties of clay. Appl Clay Sci 2016;132–133:722–30. https://doi.org/10.1016/j.clay.2016.08.029.

[33] Gu K, Jin F, Al-Tabbaa A, Shi B, Liu J. Mechanical and hydration properties of ground granulated blastfurnace slag pastes activated with MgO-CaO mixtures. Constr Build Mater 2014;69:101–8. https://doi.org/10.1016/j.conbuildmat.2014.07.032.

[34] Aldaood A, Bouasker M, Al-Mukhtar M. Effect of water during freeze-thaw cycles on the performance and durability of lime-treated gypseous soil. Cold Reg Sci Technol 2016;123:155–63. https://doi.org/10.1016/j.coldregions.2015.12.008.

[35] Eyo EU, Abbey SJ, Ngambi S, Ganjian E, Coakley E. Incorporation of a nanotechnology-based product in cementitious binders for sustainable mitigation of sulphate-induced heaving of stabilised soils, Engineering Science and Technology, an. International Journal 2021;24:436–48. https://doi.org/10.1016/j.jestch.2020.09.002.

[36] Al-Mukhtar M, Lasledj A, Alcover JF. Lime consumption of different clayey soils. Appl Clay Sci 2014;95:133–45. https://doi.org/10.1016/j.clay.2014.03.024.

[37] Vitale E, Deneele D, Russo G, Ouvrard G. Short-term effects on physical properties of lime treated kaolin. Appl Clay Sci 2016;132–133:223–31. https://doi.org/10.1016/j.clay.2016.04.025.

[38] Al-Mukhtar M, Lasledj A, Alcover JF. Behaviour and mineralogy changes in lime-treated expansive soil at 20°C. Appl Clay Sci 2010;50:191–8. https://doi.org/10.1016/j.clay.2010.07.023.

[39] Al-Mukhtar M, Lasledj A, Alcover JF. Behaviour and mineralogy changes in lime-treated expansive soil at 50°C. Appl Clay Sci 2010;50:199–203. https://doi.org/10.1016/j.clay.2010.07.022.

[40] Konan KL, Peyratout C, Smith A, Bonnet JP, Rossignol S, Oyetola S. Comparison of surface properties between kaolin and metakaolin in concentrated lime solutions. J Colloid Interface Sci 2009;339:103–9. https://doi.org/10.1016/j.jcis.2009.07.019.

[41] Choobbasti AJ, Kutanaei SS. Microstructure characteristics of cement-stabilized sandy soil using nanosilica, Journal of Rock Mechanics and Geotechnical. Engineering 2017;9:981–8. https://doi.org/10.1016/j.jrmge.2017.03.015.

[42] A.K. Jha, P. v. Sivapullaiah, Physical and strength development in lime treated gypseous soil with fly ash — Micro-analyses, Appl Clay Sci. 145 (2017) 17–27. 10.1016/j.clay.2017.05.016.

[43] Aldaood A, Bouasker M, Al-Mukhtar M. Mechanical Behavior of Gypseous Soil Treated with Lime. Geotech Geol Eng 2021;39:719–33. https://doi.org/10.1007/s10706-020-01517-w.

[44] Behnood A. Soil and clay stabilization with calcium- and non-calcium-based additives: A state-of-the-art review of challenges, approaches and techniques. Transp Geotech 2018;17:14–32. https://doi.org/10.1016/j.trgeo.2018.08.002.

[45] Firoozi AA, Guney Olgun C, Firoozi AA, Baghini MS. Fundamentals of soil stabilization. Int J Geo-Eng 2017;8. https://doi.org/10.1186/s40703-017-0064-9.

[46] A.K. Jha, P. v. Sivapullaiah, Volume change behavior of lime treated gypseous soil - influence of mineralogy and microstructure, Appl Clay Sci. 119 (2016) 202–212. 10.1016/j.clay.2015.09.017.

[47] P. Beetham, T. Dijkstra, N. Dixon, P. Fleming, R. Hutchison, J. Bateman, Lime stabilisation for earthworks: A UK perspective, Proceedings of the Institution of Civil Engineers: Ground Improvement. 168 (2015) 81–95. 10.1680/grim.13.00030.

[48] Puppala AJ, Talluri N, Chittoori BCS. Calcium-based stabiliser treatment of sulfate-bearing soils. Proceedings of the Institution of Civil Engineers - Ground Improvement 2014;167(3):162–72.

[49] Buttress A. Physicochemical Behaviour of Artificial Lime Stabilised Sulfate Bearing Cohesive Soils. University of Nottingham; 2013. PhD Thesis.

[50] Seco A, del Castillo JM, Espuelas S, Marcelino S, García B. Sulphate soil stabilisation with magnesium binders for road subgrade construction. Int J Pavement Eng 2020. https://doi.org/10.1080/10298436.2020.1825711.

[51] Wang J, Liu M, Wang Y, Zhou Z, Xu D, Du P, et al. Synergistic effects of nano-silica and fly ash on properties of cement-based composites. Constr Build Mater 2020; 262. https://doi.org/10.1016/j.conbuildmat.2020.120737.

[52] Goodarzi AR, Movahedrad M. Stabilization/solidification of zinc-contaminated kaolin clay using ground granulated blast-furnace slag and different types of activators. Appl Geochem 2017;81:155–65. https://doi.org/10.1016/j.apgeochem.2017.04.014.

[53] Suraneni P, Weiss J. Examining the pozzolanicity of supplementary cementitious materials using isothermal calorimetry and thermogravimetric analysis. Cem Concr Compos 2017;83:273–8. https://doi.org/10.1016/j.cemconcomp.2017.07.009.